Preprint
UCRL-JC-140201

High-NA Camera for an EUVL Microstepper

L. C. Hale, R. M. Hudyma, J. S. Taylor, R. L. Thigpen, and C. A. Chung

This article was submitted to
15th Annual American Society for Precision Engineering, Scottsdale, Arizona, October 22-27, 2000

September 1, 2000

U.S. Department of Energy

Lawrence
Livermore
National
Laboratory

High–NA Camera for an EUVL Microstepper

Layton C. Hale, Russell M. Hudyma, John S. Taylor, Richard L. Thigpen, Carl A. Chung
Lawrence Livermore National Laboratory, Livermore, CA 94550

Introduction

Extreme ultraviolet lithography (EUVL) is a promising next-generation technology for extending the ability of microelectronics manufacturers to make ever denser circuits with smaller features, a trend known as Moore's Law. A major EUVL program, involving three national laboratories and members of an industrial consortium,* is underway to demonstrate full-field scanned printing with 70 to 100 nm feature sizes using a four-mirror camera with a modest 0.1 numerical aperture (NA).[1] Within our program, a complementary project sponsored by International Sematech will provide an important capability to print 30 nm features using a two-mirror 0.3 NA small-field camera, see Figure 1. Known as the Micro-Exposure Tool (MET), this development tool will enable high-resolution printing several years before high-NA, pre-production (or beta) tools are available.

EUV systems operate at a much shorter wavelength than current and proposed deep-ultraviolet systems, for example, 13.4 nm versus 157 nm. This allows proportionally better optical resolution, which is often estimated using Equation 1, where k_1 is a constant related to process parameters and the source coherence, and λ is the wavelength. The NA, defined as the sine of the half cone angle of light exiting the camera, is an important optical design parameter that will likely be between 0.2 and 0.3 for EUVL production tools. Increasing the NA improves resolution but the depth of focus decreases even faster, indicated by Equation 2. Results from EUVL printing experiments lead to these estimates for the constants: $0.5 < k_1 < 0.7$ and $k_2 \approx 1$.

$$R = \frac{k_1 \lambda}{NA} \tag{1}$$

$$DOF = \pm \frac{k_2 \lambda}{NA^2} \tag{2}$$

The high absorption of EUV light in optical materials requires the use of reflective optics within a vacuum environment. This is a major departure from traditional optical lithography, which predominantly uses refractive optics. The multilayer coating technology developed within our program provides adequate reflectivity approaching 70% for normal-incidence optics, and the coating uniformity is within budgeted figure tolerances. However, the production of optical substrates to sub-nanometer figure and finish remains extremely challenging now and into the future.

Carl Zeiss is the optical fabricator contracted to produce two sets of MET optics using their own interferometers. We will install the optics into two LLNL-designed cameras and return them to Zeiss for optical system alignment. Zeiss will assume ownership of one camera for their internal use and the other will eventually be installed into the MET.†

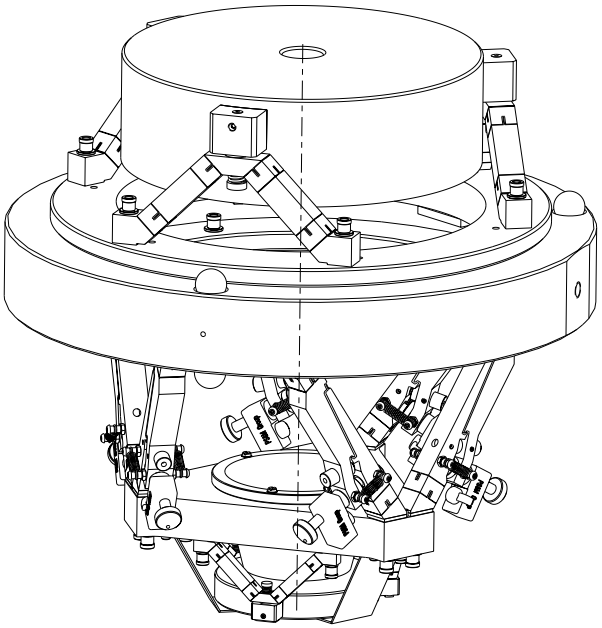

Figure 1 Solid model of the MET camera design.

Overview of the Optical Design

The MET camera employs two mildly aspheric mirrors: a convex primary (designated M1) and a concave secondary (designated M2) having nearly the same radius of curvature. This "equal radii" concept enables the field curvature to be corrected to a value significantly better than other two-mirror cameras such as the Sandia 10x camera, a Schwarzchild configuration.[2] As Figure 2 shows, each optic has a central hole to permit ray bundles to pass through. The optical design is rotationally symmetric about the optical axis except for 4° and –0.8° tilts of the mask and wafer planes, where

This work was performed under the auspices of the U.S. Department of Energy by University of California, Lawrence Livermore National Laboratory under contract No. W-7405-Eng-48.

* The Virtual National Laboratory (VNL) is a cooperative partnership between Sandia National Laboratory, Lawrence Berkeley Laboratory and Lawrence Livermore National Laboratory. The Limited Liability Company (LLC) is a consortium of microelectronics manufacturers who sponsor and participate in EUVL research.

† At the time of this writing, the optics and camera hardware are nearing completion. Full assembly is anticipated by the publish date with optical alignment to follow. The Micro–Exposure Tool is just entering the conceptual design phase. The MET will be located in the US.

the ratio is equal to the 5:1 magnification. Tilted planes are required when using a reflection mask in the way anticipated for EUVL production tools. In this case, the field size projected onto the x-y plane is 3 x 1 mm at the mask and 600 x 200 μm at the wafer.

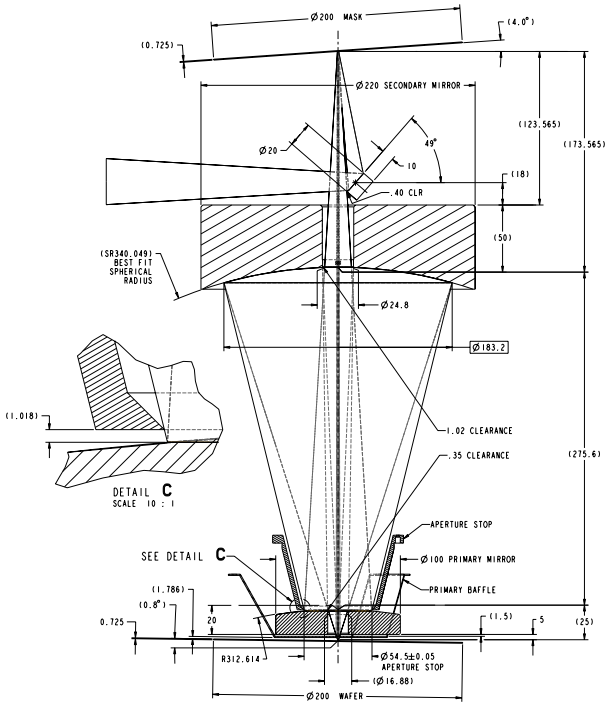

Figure 2 Cross section of optical components with all ray bundles shown. The dimensions are in millimeters.

While the wavefront error is well corrected for tilted planes, the magnification varies across the tilted field, resulting in significant image distortion. However, distortion is not a concern for the process development studies planned for the MET. Without tilted planes, the MET camera may be used with a transmission mask for printing devices that require low distortion. Table 1 summarizes the errors inherent to the optical design, that is, assuming perfect optics. Figure errors on the optics cause twice the error in reflected wavefront and are assumed to combine in quadrature. Since several low-order error functions are compensable at system alignment, quadrature becomes a realistic assumption.

Error Type	Tilted	Not Tilted
Composite RMS Wavefront	0.42 nm	0.28 nm
Maximum RMS Wavefront	0.72 nm	0.36 nm
Minimum RMS Wavefront	0. 24 nm	0.15 nm
Peak Distortion	242 nm	2.24 nm

Table 1 Errors inherent to the optical design computed over the full 600 x 200 μm wafer field.

Optic Specification

The optic specification for the MET is identical to that of the four-mirror camera mentioned previously.[3] The advantage of fewer optical surfaces in the MET is partially offset by the more stringent printing requirements for 30 nm. The specification comprises three measures of surface error integrated over consecutive regimes of spatial frequency as listed in Table 2. These are tied closely to performance requirements and the bandwidth of various measuring instruments. The figure specification relates to high-resolution, low-distortion imaging across the full field. Figure error is measured using full-aperture interferometry. MSFR (mid-spatial-frequency roughness) causes near-angle scattering such that the scattered light remains in the image field. MSFR causes background illumination superimposed on the desired image, thus reducing image contrast and process window. In addition, nonuniform contrast over the image field causes the critical dimension of printed features to vary over the field. MSFR is measured using phase-shifting interference microscopy with several objectives to cover the frequency range. HSFR (high-spatial-frequency roughness) scatters light outside the image field, thus reducing throughput and also decreasing contrast. HSFR is measured using atomic force microscopy.

Error Regime	Specification	Spatial Period
Figure	0.25 nm rms	> 1 mm
MSFR	0.20 nm rms	1 mm – 1 μm
HSFR	0.10 nm rms	< 1 μm

Table 2 Specifications for MET projection optics.

The degree of difficulty in meeting the figure and MSFR specification depends largely on the asphericity of the optics. The peak aspheric departure for the smaller M1 is reasonable at 3.82 μm but the maximum aspheric slope is rather large at 1.18 μm/mm. The peak aspheric departure for M2 is 5.61 μm with a maximum aspheric slope of 0.47 μm/mm. The substrates are Zerodur™ to minimize thermal distortion.

Functional Requirements of the Camera Body

The camera body must satisfy three functional requirements extraordinarily well: 1) low-distortion support of the optics, 2) precision adjustments for aligning the optics, and 3) dimensional stability, both long term for alignment and short term for image placement. In addition, the camera must function in a vacuum environment and define the boundaries of ray bundles passing through it.

Description of Structural Components

Figure 1 shows the complete camera design from which the key structural components are visible. The support ring provides upper and lower kinematic mounting interfaces available to the MET and the alignment interferometer. In addition, the support ring has a 360° rotational interface to the M2 cell for the clocking adjustment and it provides attachment points for six actuation flexures. The triangular-shaped M1 cell attaches to the opposite ends of the actuation flexures, and together they provide high-resolution adjustment in

the five degrees of freedom critical for optical alignment. The M1 and M2 cells each support three flexures that combine to constrain six degrees of freedom for each optic. In addition, the flexures each provide a quick-disconnect interface to three lugs that are permanently bonded to each optic. The support ring, actuation flexures, cells, flexures and lugs are manufactured from Super Invar, a low-CTE (coefficient of thermal expansion) alloy of iron, nickel and cobalt.

Aperture Stop and Baffles

The boundaries of ray bundles through the camera are controlled by the aperture stop on the outer dimensions and a pair of baffles on the inner dimensions. As Figure 2 shows, the aperture stop is located just above optic M1 and is easily replaced if there is an experiment need to change its size. The purpose of the baffles is to block the direct light path from mask to wafer allowed by the central holes in the optics. The hole baffle, located below M1 and above the wafer, reduces the effective size of a direct ray bundle from the 16.6 mm hole size through M1 to just 4 mm. The plug baffle, located and attached via a single cantilever to the central hole area in optic M2, actually blocks the direct ray bundle. The hole and plug baffles combine to block all light emanating within a 4 mm circle on the mask.

Optic Mounts

The optic mounts must reproduce the same optic figure in the camera as achieved during fabrication metrology, within about 10% of the optical figure specification. We could not reasonably use the camera mount also for fabrication metrology due to space constraints within the interferometer. Instead, separate metrology mounts for M1 and M2 were constructed to provide a constraint state nominally identical to the respective camera mounts. Each mount is kinematic providing exactly six constraints that fully arrest the degrees of freedom of the optic without overconstraint. Neglecting friction, each mount carries the weight of the optic through three points that are geometrically defined at the centers of spherical surfaces on the bonded lugs. The reaction force at each point is nominally vertical but may vary due to friction, manufacturing tolerances in the mounts and misalignment to the gravity vector. The error budget process identified sliding friction as a significant error source to contend with in the mount designs.

The camera mount uses three, two-constraint flexures to support each optic. The flexures are arranged as three vees with their vertices coincident with spherical interfaces each formed between a conical seat on the flexure and the spherical surface on the bonded lug. This arrangement is evident in Figure 1. The optic is placed in the mount with full freedom to align to the mount constraints while minimizing sliding friction at the sphere-cone interfaces. Once fully constrained in the mounts, preload springs are applied in a way that does not disturb the interfaces. The metrology mount duplicates the same constraints as the camera mount using rolling-element bearings to reduce fiction to an acceptable level. Figure 3 shows the M1 metrology mount and the M2 metrology mount is similar.

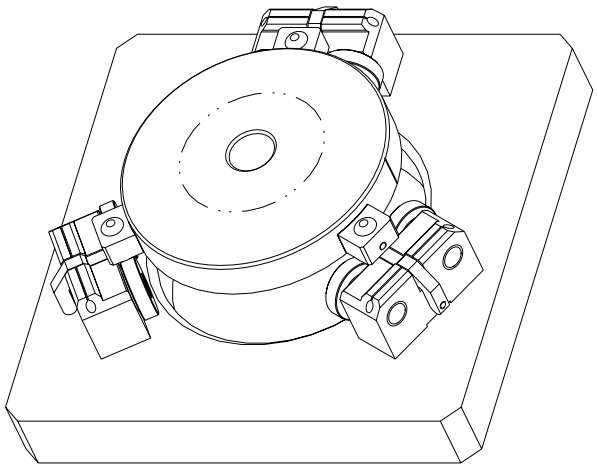

Figure 3 The M1 metrology mount uses pairs of rolling-element bearings to form a three-vee kinematic coupling.

Actuation System

The actuation system shown in Figure 1 has six actuation flexures that support and move the M1 optic and cell relative to the support ring. Often called a Stewart platform, this type of system is classified as a parallel-link mechanism since the active members act as structures in parallel as opposed to serial or stacked actuation stages. All six members are required to provide rigid constraint, and any pure motion of the stage requires coordinated motion of all six flexures. The coordination may be described with sufficient precision using a linear matrix equation since the required motions are small with respect to the overall size of the links.

The range and resolution requirements flow down from optical alignment needs. Table 3 summarizes the requirements and the capability of the actuation system. The actuator resolution for x-y translation is set to match the need to affect the transmitted wavefront at the 0.05 nanometer level. The geometry of the actuation system is such as to surpass the need in the other degrees of freedom. The most significant margin is in z translation because the interferometer will refocus as part of the alignment, thus relaxing the actuation requirement. However, this direction is the most sensitive for stability of the focal plane. The required alignment range comes from a Monte-Carlo simulation using anticipated manufacturing tolerances. It was reasonable to provide an actuator range having nearly a 5x margin. This requires the dynamic range of the sensors to be 4000:1 or 12 bits. The actuation system is capable of somewhat larger moves in single directions than those stated in Table 3. A three-way RSS combination: ±150 μm Δx-Δy, ±100 μm Δz, ±1000 μr θx-θy, uses the full ±149 μm travel of one or more actuation flexures.

Stage Motion	0.05 nm Sensitivity	Actuator Resolution	Tolerance Model	Actuator Range
Δx	0.10 μm	0.10 μm	± 34 μm	± 150 μm
Δy	0.10 μm	0.10 μm	± 34 μm	± 150 μm
Δz	0.61 μm	0.05 μm	± 21 μm	± 100 μm
θx	1.20 μr	0.80 μr	± 120 μr	± 1000 μr
θy	1.20 μr	0.80 μr	± 120 μr	± 1000 μr

Table 3 Range and resolution for actuated degrees of freedom.

Actuation Flexure

The function of the actuation flexure is to provide a single, adjustable constraint along its axis. It is remotely actuated during alignment corrections but otherwise functions as a passive constraint. Figure 4 is a cross section through the actuation flexure that shows the piezo-screw actuator and LVDT position sensor. A computer controller closes the loop on each actuator and computes the decoupling relation for coordinated motion. Effectively the piezo-screw actuator operates an 11:1 lever that is cut into the actuation flexure.

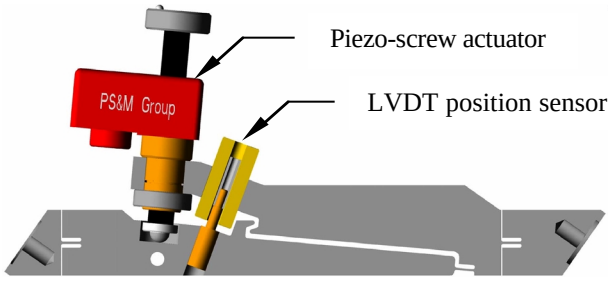

Figure 4 The section shows three of five blade flexures formed by a series of EDM cuts. The two blades near each end have identical companions that are rotated 90˚ about the constraint axis and are not visible in the section. Each pair acts as a ball joint. The single off-axis blade allows the flexure freedom to actuate within the travel stop. The screw axis, the constraint axis and a straight-line extension of the off-axis blade all intersect at a common point.

A number of factors are considered and balanced in the design of the actuation flexure. It must provide stiff axial constraint, sufficient compliance and range of motion in the non constraint directions, low actuation force, and bending stresses below yield. The axial stiffness governs the modal frequencies associated with the M1 optic and cell. Modes of vibration within the flexure, so called flexure modes, are of little consequence because associated optic motion is second order. However, the desire to keep these frequencies relatively high (> 200 Hz) limits the flexibility of the blades and ultimately the travel and lever ratio of the actuator.

A finite element analysis of the actuation flexure shows that the maximum actuation force and bending stress are 2.74 N and 178 MPa, respectively, which are within the design constraints. The total compliance along the constraint axis is 37.85 nm/N and is fairly well distributed with the lever arm and column being the greatest contributors. Both could easily be made stiffer but the increased mass would lower the flexure-mode frequencies, particularly the torsional mode at 250 Hz (not including the actuator or LVDT in the model). Further gains could be made by optimizing individual blade flexures for their expected ranges of travel, but instead they were all given the same proportions: 0.5 mm thick, 16 mm wide and 5 mm long.

Dynamic System Modeling

The need for steady image placement over the length of an exposure drives the dynamic stability requirement to be only a few nanometers of relative motion. Since the MET tool body and vibration isolation system heavily influence the performance of the whole lithography system, the strategy used in the camera design has been to maximize modal frequencies involving optic motion, thus deferring rigorous dynamic response modeling to the full MET system design.

A fairly detailed finite element model was developed to obtain the modal analysis results given in Table 4. Two boundary conditions were considered: 1) rigid kinematic constraints to identify flexibility within the camera assembly; and 2) kinematic constraints with modeled compliance to estimate a realistic system response. For the rigid case, optic M2 is the first to show motion at 353 Hz followed by M1 at 418 Hz. On real kinematic mounts, the camera moves nearly as a rigid body at 208 Hz.

Mode No.	Frequency	Mode Shape Description
Results for a rigid kinematic constraint		
1-6	250 Hz	Torsion of actuation flexures
7-12	344 Hz	Torsion of M2 flexures
13 & 14	353 Hz	X-Y motion of M2
15 & 16	418 Hz	X-Y motion of M1 optic/cell
17	525 Hz	Z motion of M2
18 & 19	530 Hz	Combined X-Y, θ_x-θ_y motion
Results for a compliant kinematic constraint		
1 & 2	208 Hz	Nearly rigid X-Y motion, all
9 & 10	310 Hz	Nearly rigid θ_x-θ_y motion, all

Table 4 Summary of the modal analysis results for rigid kinematic constraints and also three-vee kinematic constraints assuming silicon nitride as the ball material and tungsten carbide as the vee material.

References

1 Tichenor, Daniel A., et al., "EUV Engineering Test Stand," SPIE Emerging Litographic Technologies IV, 2000, **3997**

2 Goldsmith, J. E. M., et al., "Sub-100 nm Imaging with an EUV 10x Microstepper," SPIE Emerging Litographic Technologies III, 1999, **3676**

3 Taylor, Sommargren, Sweeney, Hudyma, "The Fabrication and Testing of Optics for EUV Projection Lithography" *Proc ASPE*, 1998, **18**